Dynamics of dust particles confined in imposed potential structures in strongly magnetized, low-temperature plasmas

Taylor Hall [*] and Edward Thomas, Jr.
Department of Physics, Auburn University, Auburn, Alabama 36849, USA

(Received 22 March 2020; revised 17 July 2020; accepted 24 July 2020; published 17 August 2020)

A new phenomenon called imposed ordered structures has been of particular interest to the dusty plasma community within the past several years. These structures are a new type of pattern formation within a dusty plasma in which the dust particles become fixed to a background confining potential whose spatial structure is determined by some conducting element present in the plasma. In previous works, this element has typically been a conducting wire mesh. One of the unanswered questions is whether the dust particles become trapped beneath the conducting surface of the mesh or in the gaps (holes) between the wires. This work makes use of a new electrode whose shape is designed to mimic that of wire mesh, but with much larger dimensions to facilitate *in situ* diagnostic measurements. Observations of the dust show that particles become confined to the regions beneath the holes of this new electrode. Measurements of the dust particle velocities allow for a determination of the kinetic energy within the dust cloud which show that the particles are in an energetic steady state. Comparisons of spatial profiles of the particle velocities also show that the dust particles typically reside in areas of increased plasma glow, possibly being trapped by plasma filaments.

DOI: 10.1103/PhysRevE.102.023208

I. INTRODUCTION

A complex, or dusty, plasma is a four-component plasma system consisting of ions, electrons, neutral gas atoms, and charged microparticles called dust particles or grains [1–3]. These microparticles become charged through the collection of ions and electrons from the background plasma [4–6]. Dust particles in a laboratory plasma setting acquire a net negative charge due to the electrons having a higher mobility than the ions. This charge can range from a few hundred electron charges to tens of thousands of electron charges depending on the dust grain radius. Once charged, the dust grains become coupled to the background plasma and act as an additional plasma component. In a laboratory, dusty plasmas are most often created in a low-temperature plasma whose electrons have a temperature between 2 and 5 eV and with ions that are at room temperature of 0.025 eV. Electron and ion densities within these plasmas are typically on the order of 10^{15} m^{-3}.

In the past several years, a new phenomenon within the field of dusty plasmas called imposed ordered structures has been discovered. This phenomenon is observed as a new type of pattern formation within a dusty plasma in which dust particles become spatially aligned to a fine wire mesh, whose spatial dimensions were comparable to the electron Debye length and the ion gyroradius (i.e., ∼300–600 μm), that is placed at the boundary of the plasma. These structures occur at high magnetic fields ($B \geqslant 1$ T) and were first reported in the Magnetized Dusty Plasma Experiment (MDPX) [7] at Auburn University. In these experiments, the dust grains were organized into a square lattice pattern whose interparticle spacing matched those of a conducting wire mesh which was situated in one of the plasma-generating electrodes.

The initial observations found that these imposed ordered structures required that the conducting element present in the plasma have some distinct pattern. As shown in Fig. 4 of Ref. [7], when the conducting wire mesh was partially covered with conducing glass only the uncovered section was able to generate the structures within the dust cloud. Additionally, those experiments found that the structures required low neutral gas pressures in addition to high magnetic fields. With increasing neutral pressure, the increased collisionality with the neutrals was postulated to lead to the dissipation of these potential structures and an eventual loss of the imposed pattern.

Follow-up experiments by Thomas *et al.* examined the behavior of particle motion within the imposed ordered structures [8]. In this work, the dynamics of particle hopping, as well as particles trapped at discrete locations within the imposed ordered structure, was investigated to determine the structure of the electric potential barrier that either impeded or bound particles within the dust cloud. Additional experiments reported by Hall *et al.* were performed to measure a bond order parameter and average light intensity which provide a method to quantify the experimental conditions at which the imposed ordered structures appear [9]. That work found strong evidence that the onset of the imposed ordered structures was correlated to an increase in the plasma magnetization, described by the modified ion Hall parameter

$$h' = \frac{\lambda_{mfp}^{in}}{2\pi r_{Li}} \sim \frac{B}{P}, \tag{1}$$

where λ_{mfp}^{in} is the ion-neutral mean free path, r_{Li} is the ion Larmor radius, B is the magnetic field, and P is the neutral gas pressure.

[*]Corresponding author: thh0006@auburn.edu

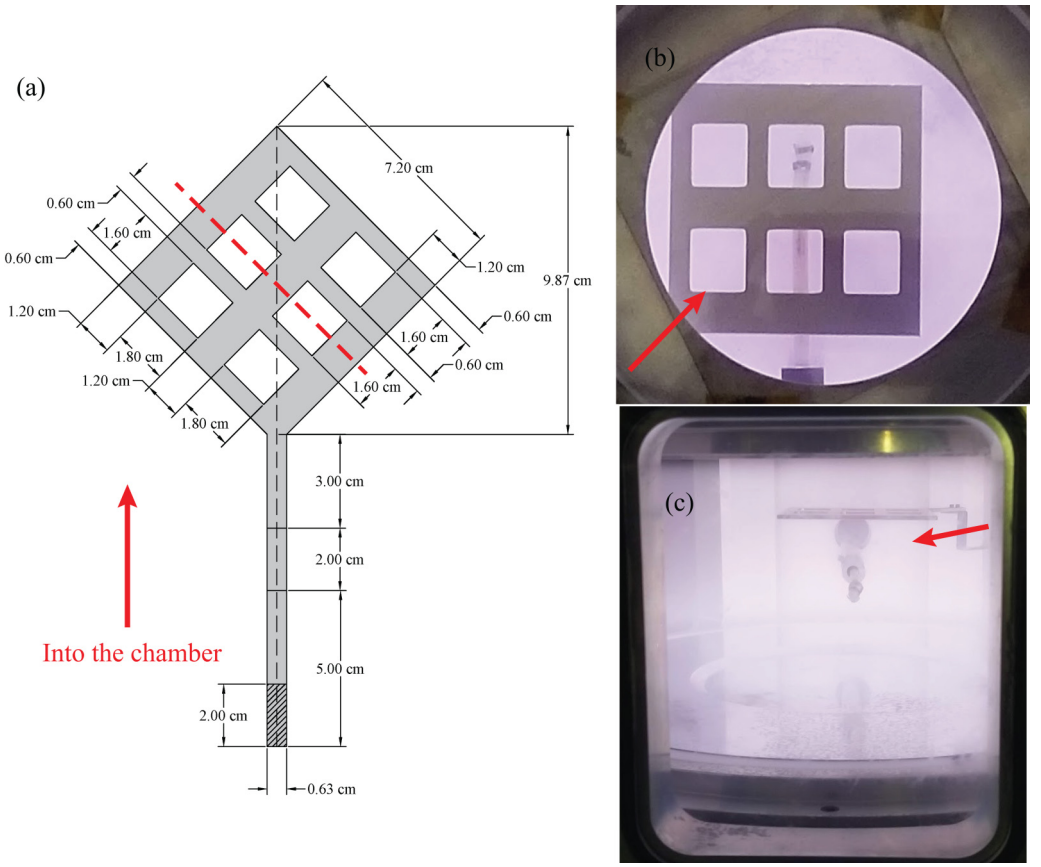

FIG. 1. (a) Top schematic view of the gridlike waffle electrode. The red dashed line indicates the line at which the vertical laser sheet intersected the waffle electrode. (b) Top down view of the waffle electrode within the vacuum chamber. A plasma probe can be seen beneath the grid. (c) Side view of the waffle electrode in the vacuum chamber. The red arrow in each part indicates the direction into the center of the chamber to orient each of the parts.

One of the open questions from those previous experiments is whether the dust is trapped beneath the conducting wire section of the mesh or between the holes in the space between the wires. This question was difficult to answer due to the physical limitations of the imaging systems used to record the dust particles and due to the fact that with the small square mesh, the spacing between the wires and the spacing between the centers of the holes in the mesh pattern are identical. In those earlier experiments, the wire mesh was small enough (wire dimension less than or equal to 1 mm) and far enough from the focal plane of the camera (greater than 2 cm) that the trapping location of the dust particles relative to the mesh could not be resolved in the recorded videos. These small wire dimensions also severely limited the ability to use plasma probe diagnostics for measuring the spatial variation of plasma parameters such as temperature and density, which could be used for investigating imposed ordered structures.

To address these limitations, this work will instead make use of a larger waffle-shaped electrode, a schematic of which is shown in Fig. 1, to create the imposed ordered structures. This electrode has several key differences from the wire mesh. The first is that the scale of this electrode is several hundred times larger than the wire mesh, having conducting elements on the order of 1 cm in size. Where the wire diameter in the original mesh experiments was on the order of the plasma Debye length, the "waffle" electrode is tens to hundreds of times larger than the usual length scales within the plasma (the Debye length, ion or electron mean free paths, ion or electron Larmor radii, etc.) The aspect ratio of the conducting elements to the spacing between those elements is also different for the waffle electrode. For the wire mesh the spacing was twice the diameter of the wire, and for the waffle electrode this spacing is variable depending on which direction the electrode is viewed from. For the experiments presented here the gap between elements is only 50% larger than the conducting elements. How the scaling of these two characteristic features of the conducting hardware which produces the imposed ordered structure will not be examined in this work.

The benefit of this larger design will be that it is immediately clear where the dust particles become trapped beneath the electrode. Because of the drastically altered scale of this electrode, the behavior of the dust particles and development of a confining potential structure may differ from observations made using the smaller wire mesh. The large spatial dimensions of this experimental configuration will allow measurements of the dust particle velocities to be performed. These measurements will then be used to show that the dust particle system is in an energetically steady state. Spatial profiles of the particle velocities will also be compared to observations of the plasma glow, which may indicate that dust particles are drawn towards regions beneath the waffle electrode which contain a higher number of plasma filaments.

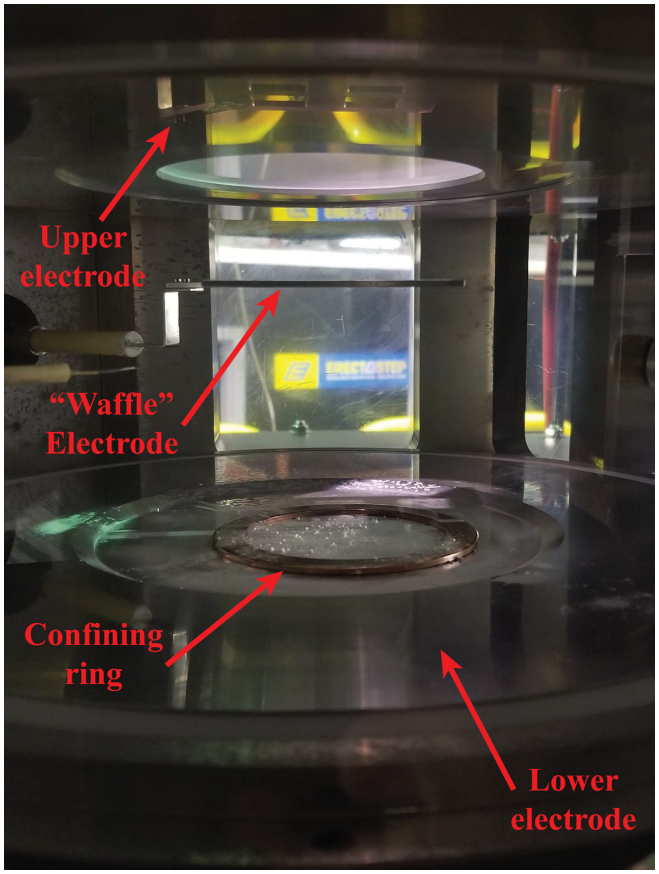

FIG. 2. Internal configuration of the vacuum chamber. The top and bottom rf electrodes are shown, as well as the waffle electrode and the ring used to confine dust particles. A coating of residual dust particles can also be seen within the confining ring.

II. EXPERIMENTAL SETUP

The MDPX is a split-bore, multiconfiguration, superconducting magnet device, capable of producing up to 4-T magnetic fields at its center. The magnet system consists of four magnet coils, housed in a split-bore cryostat with two coils in each of the halves. The experimentally accessible warm bore is a cylindrical region 50 cm in diameter and 157 cm in length. The design and capabilities of the MDPX have been described extensively in previous literature and the description presented here will focus of the aspects of the magnet and vacuum systems which are relevant to the work presented here [10–12].

The experiments performed for this work were carried out in the primary MDPX octagonal vacuum chamber. Capacitively coupled, radio-frequency-generated argon plasmas are generated within the vacuum vessel using a pair of electrodes that are shown in Fig. 2. The electrodes are 34.2 cm in diameter at the top and bottom of the chamber. For the experiments described here, the rf is 13.56 MHz and has an input power of 5 W. The powered bottom electrode has a 15.2-cm-diam, 0.3-cm-deep depression in the center and the electrically floating top electrode has a 14.6-cm-diam through hole for optical access along the magnetic axis. This through hole was covered with a square of fluorine-doped tin-oxide-coated glass with the nonconducting side facing downward toward the plasma to mimic the nonconducting boundary above the conducting mesh in earlier experiments.

Experiments were conducted for a range of background neutral pressures of $P = 25$–75 mTorr (3.33–10.0 Pa). The magnetic fields used ranged from $B = 0.00$ to 2.05 T. Measurements made with a double Langmuir probe [13,14] were used to measure the background electron temperature within the plasma, which was found to generally be on the order of 3.2 ± 0.5 eV. The waffle electrode, seen inside the vacuum vessel in Fig. 2, is a 0.64-cm-thick aluminum square of 7.2 cm on each side with six $1.6 \times 1.8\,\mathrm{cm}^2$ rectangular holes giving the electrode its waffle design. The electrode was placed into the center of the vacuum chamber on an aluminum rod within a ceramic tube and an S-shaped arm which placed the electrode 8.25 cm above the bottom electrode. An electrical bias of ± 40 V was applied to the electrode for the experiments presented here.

Silica dust particles with dust radius $a = 4 \pm 0.4$ μm were injected into the plasma via a dust shaker. Dust clouds were levitated vertically by the sheath electric field 0.5–1.5 cm above the lower electrode or 6.75–7.75 cm below the waffle electrode. A 4½ in. type copper gasket of 8.23-cm outer diameter and 6.38-cm inner diameter was placed at the center of the chamber below the waffle electrode to provide a horizontally confining electric field. For the purposes of these experiments it is assumed that the orbit-motion-limited theory [2,15] estimate of the particle charge will remain relatively constant with increasing magnetic field. It is believed that this is a reasonable assumption since the particles remain levitated within the plasma under all conditions from $B = 0.0$ to 2.05 T. The total dust charge q_d calculated from the electron temperature is given as

$$q_d = -Z_d e, \tag{2}$$

where e is the elementary charge and Z_d is the number of electrons having an average of $20\,730 \pm 2530$ electrons per dust particle.

The dust clouds in this experiment were recorded from two directions, from the side perpendicular to the magnetic axis through a view port on the chamber and from the top along the magnetic axis through a top window. For the recordings made by the side camera, a vertical plane of particles was illuminated by a 633-nm-wavelength red laser diode passed through a cylindrical lens to make a vertical sheet of laser light which intersects the waffle electrode along a centerline shown in Fig. 1(a). For the top view, particles were illuminated by a 532-nm horizontal laser sheet produced in a similar manner to the vertical laser sheet. Dust particles were recorded from both directions using a Ximea model xiQ MQ042MG-CM camera and Nikon MicroNikkor 200-mm lens. In both sets of recordings, videos of 500 total frames were recorded at 90 frames/s, with a 10-ms exposure time in the side view and a 2-ms exposure time in the top view. For the side camera the resolution of the video images was 2048 × 800 pixels with a spatial resolution of 27 μm/pixel; for the top view the resolution of the video images was 1600 ×1980 pixels with a spatial resolution of 28 μm/pixel.

III. EXPERIMENTAL OBSERVATIONS AND MEASUREMENTS

The most immediate observation from these experiments is that the dust clouds in the presence of the magnetic field were positioned beneath the holes of the waffle electrode. This is illustrated in Fig. 3. In Fig. 3(a), with a neutral gas pressure of 25 mTorr (3.33 Pa) and waffle electrode bias of −40 V, when $B = 0.0$ T, the dust particles appeared as a singular cloud, with only some small vertical motion, and spread throughout the entire region beneath the electrode. When the magnetic field was turned on it is shown that the dust resides between the conducting sections of the electrode, whose location is indicated by the red bands at the top and the vertical red dashed lines. In Figs. 3(b) and 3(c), for magnetic fields up to 1 T, the dust particles have separated into two clouds which resided beneath the holes and had a significantly increased vertical range and motion. At even higher magnetic fields $B \geqslant 1.5$ T, the dust clouds decomposed further, becoming confined to the inner edges of the hole, and no longer spanned the full horizontal range, as found in Figs. 3(d) and 3(e). This behavior was also observed for the waffle electrode bias of +40 V at 25 mTorr (3.33 Pa). For both waffle electrode biases, the separation of the dust cloud into multiple clouds residing beneath the holes at higher neutral gas pressures of 50 and 75 mTorr (6.67 and 10.0 Pa) was also observed, though it typically required higher magnetic fields, $B \geqslant 1.0$ T, to see similar effects to the 25-mTorr cases.

Video recordings of the dust particles were also used to measure the particle velocities throughout the cloud using particle image velocimetry (PIV). This approach to measuring dust particle velocities has been reported in several earlier publications [8,16–18]. In order to more accurately identify particles, videos were first processed to isolate the dust particles by removing the image background around the particles. The processed images were then analyzed using the DaVis software package from LaVision, Inc. [19] Velocity distributions of the PIV vector results were also broadened according to results by Williams and co-workers to account for PIV measurement effects on the real dust velocity distributions [20,21].

A series plot of the resulting velocity vectors is shown in Fig. 4 at a time $t = 2.0$ s into the 5.5-s-long video recording. The overall randomness of the velocity vectors indicates that there is no flow present in the particle cloud or bulk rotation of the dust cloud which was observed in previous experiments with the wire mesh. The application of PIV techniques has been discussed extensively in previous work by Thomas and co-workers [20,22–26].

The resulting velocity vectors whose location coordinates within the image which were outside some vertical bounds ($4.04\ \text{cm} < y < 16.15\ \text{cm}$) were removed as no real particles were present outside those bounds, i.e., reflections of particles on the electrode might produce vectors. Using the remaining velocities, a root mean square velocity was calculated at each spatial coordinate (i.e., interrogation cell) over the full 500-image sequence as

$$v_{\text{rms}} = \sqrt{\frac{1}{n}\left[\left(v_{x1}^2 + v_{y1}^2\right) + \left(v_{x2}^2 + v_{y2}^2\right) + \cdots + \left(v_{xn}^2 + v_{yn}^2\right)\right]}, \tag{3}$$

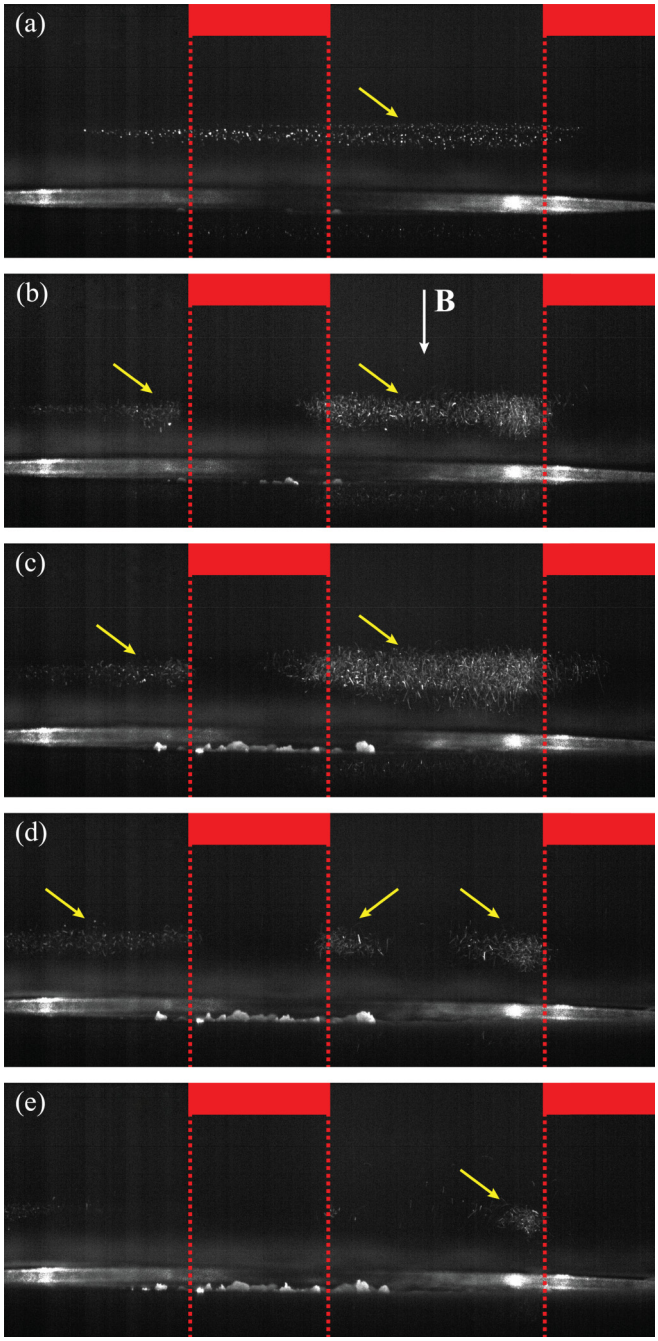

FIG. 3. Dust position beneath the waffle electrode for a neutral pressure of 25 mTorr (3.33 Pa) and a waffle electrode bias of −40 V. Magnetic fields of (a) $B = 0.0$ T, (b) $B = 0.51$ T, (c) $B = 1.02$ T, (d) $B = 1.54$ T, and (e) $B = 2.05$ T are shown and the magnetic field is directed downward in the images. The location of the conduction surface of the waffle electrode is indicated by the red bands and the top and its edges are shown by the vertical red dashed lines. Yellow areas highlight the position of the dust clouds within each image. It is clearly observed that the dust particles levitate beneath the holes of the waffle electrode.

where n is the number of valid vectors at each spatial point. The resulting v_{rms} for a neutral gas pressure of 25 mTorr (3.33 Pa) and waffle electrode bias of −40 V is shown in Fig. 5 for a range of magnetic fields. The location of the maximum

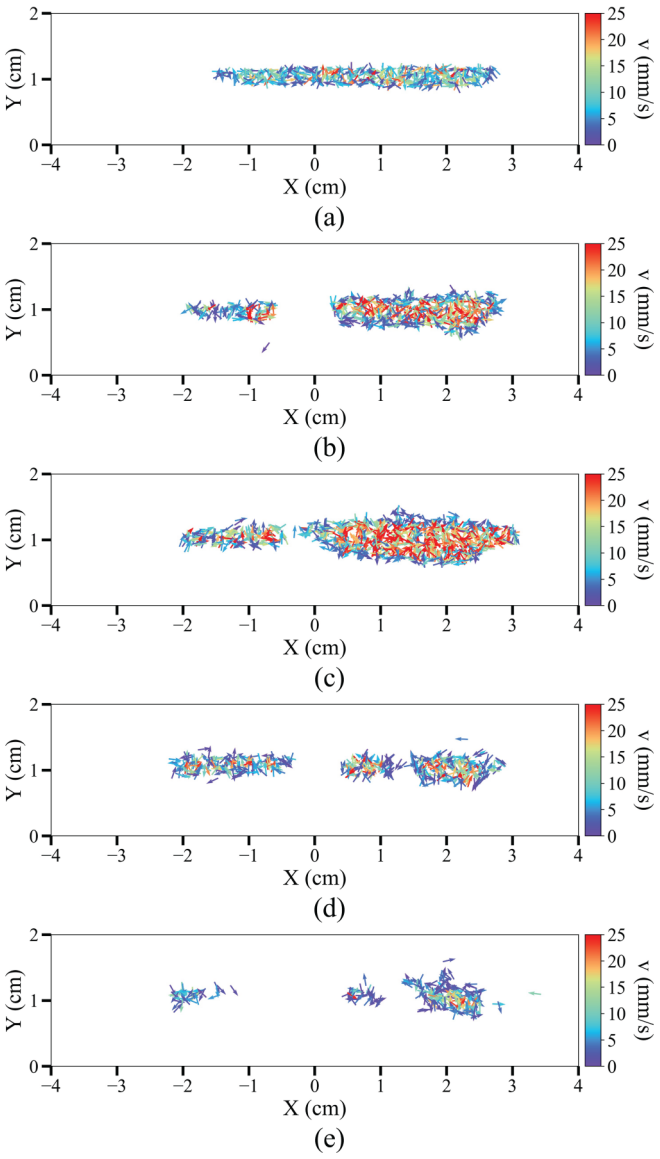

FIG. 4. Series of instantaneous velocity vector fields from PIV calculations at a neutral pressure of 25 mTorr (3.33 Pa) and a waffle electrode bias of −40 V at magnetic fields of (a) $B = 0.0$ T, (b) $B = 0.51$ T, (c) $B = 1.02$ T, (d) $B = 1.54$ T, and (e) $B = 2.05$ T, at time $t = 2.0$ **s** into the 5.5-s-long video recording. In the horizontal x direction, every sixth vector is plotted, and in the vertical y direction, every fourth vector is plotted from the full vector field. The overall randomness of the vector directions indicates that there is no flow present in the particle motion.

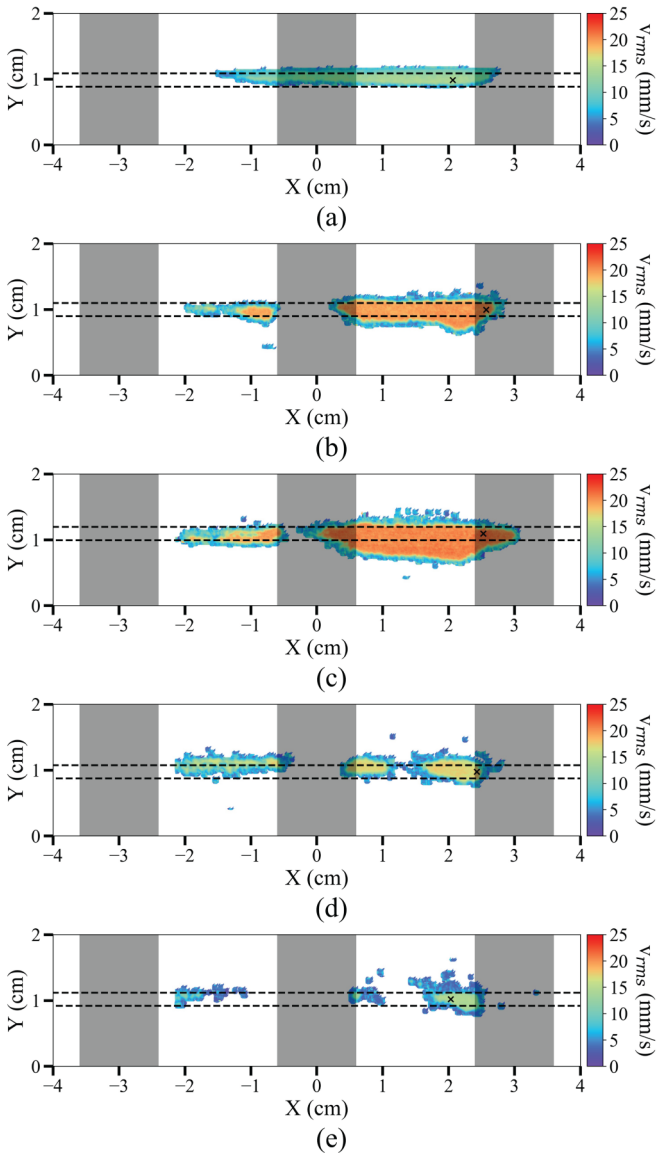

FIG. 5. Root mean square velocities of dust particles for magnetic fields of (a) $B = 0.0$ T, (b) $B = 0.51$ T, (c) $B = 1.02$ T, (d) $B = 1.54$ T, and (e) $B = 2.05$ T, all at a neutral pressure of 25 mTorr (3.33 Pa) and a waffle electrode bias of −40 V. The position of the waffle electrode is shown as vertical gray bands within the plots.

$v_{\rm rms}$ within each plot is marked by a black × and a horizontal "box" through the cloud, 0.2 cm tall, is centered vertically according to that location as indicated by the two dashed black bars in each panel of Fig. 5.

IV. DISCUSSION OF RESULTS

Dusty plasma systems have a number of conservative forces, such as electric and gravitational forces, and nonconservative forces [6,27,28], such as ion and neutral drag, acting on the system which act as energy sources or sinks. To examine if any force imbalance exists within the dusty plasma system, an examination of the average kinetic energy of the system is made. Here the average dust kinetic energy is calculated as

$$K_{\rm trans} = \tfrac{1}{2} m_d \langle v_x^2 + v_y^2 \rangle = \tfrac{1}{2} m_d \langle v_{\rm rms}^2 \rangle, \tag{4}$$

where m_d is the mass of a dust particle and $\langle v_{\rm rms}^2 \rangle$ is the average $v_{\rm rms}$ squared in each frame. When plotted as a function of time, as shown for a variety of electrode biases and magnetic fields in Fig. 6, $K_{\rm trans}$ is found to be effectively constant with only some small variations. Here $K_{\rm trans}$ is normalized to the mean translational kinetic energy $\bar{K}_{\rm trans}$. This allows for the relative variation among parameter combinations to be more apparent. This mean kinetic energy and the associated standard deviation are given in each panel.

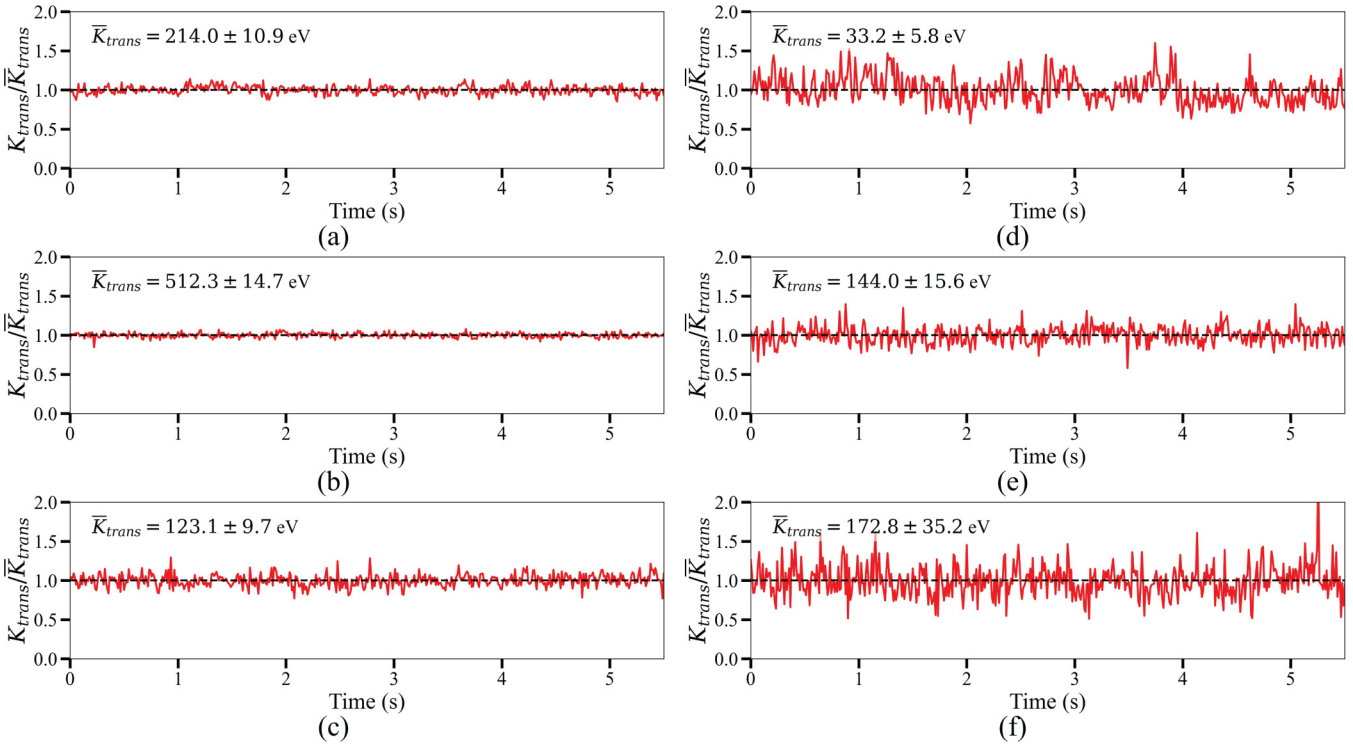

FIG. 6. Plots of the average dust kinetic energy normalized to the mean kinetic energy within each frame as a function of time. The three rows show the kinetic energy at increasing magnetic fields B: (a) and (d) $B = 0.0$ T, (b) and (e) $B = 1.02$ T, and (c) and (f) $B = 2.05$ T. The two columns show results for different combinations of neutral gas pressures P and waffle electrode bias V: (a)–(c) $P = 25$ mTorr and $V = -40$V and (d)–(f) $P = 75$ mTorr and $V = +40$ V. The systems, regardless of magnetic field, neutral pressure, or waffle electrode bias, appear to remain steady in time. Higher-pressure conditions, such as those in (d)−(f), typically have a much lower average kinetic energy and have a much higher variance relative to the average.

From these observations, no change in kinetic energy over time is found and the system can be taken to be in a steady state. This result could also be interpreted as meaning that there is no significant force imbalance within the dust cloud. So, while there certainly are drag effects acting on the system, they are sufficiently balanced by restorative forces such as the electric fields or other sources of energy from the background plasma.

The time-averaged kinetic energy is shown in Fig. 7(a) and better illustrates some of the trends seen in Fig. 6. Most notable is that the average kinetic energy decreases with an increase in neutral gas pressure. Regardless of pressure or electrode bias, the energy appears to exhibit similar trends with magnetic field, quickly peaking around $B = 0.5$ T and slowly decreasing at higher magnetic fields. The ratio of standard deviation in time to the time-averaged kinetic energy is shown in Fig. 7(b). While the highest neutral pressure cases have the lowest kinetic energy per vector, they consistently have much higher variances. This is likely due to the smaller dust cloud size at these conditions, which reduces the vector sample size. For lower pressure cases, 25 and 50 mTorr (3.33 and 6.67 Pa), this ratio is quite low, typically less than 10%, further supporting the argument that the system is in a steady state.

As reported previously, one of the most significant observations from these experiments is that the dust particles were found to accumulate beneath the holes of the waffle electrode at higher magnetic fields. In Fig. 8, profiles of the root mean

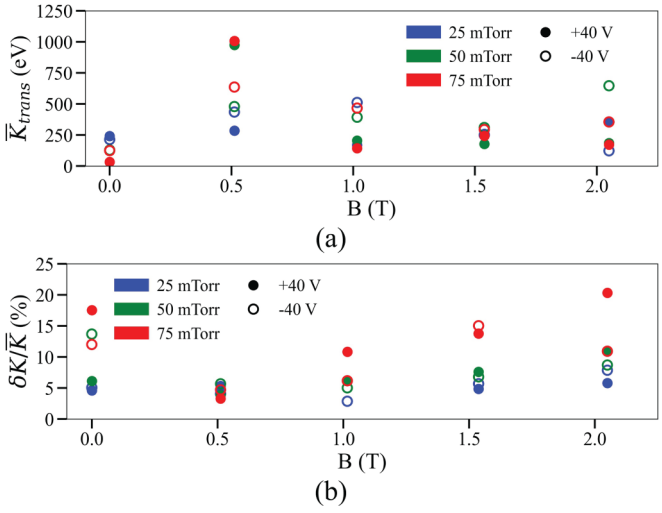

FIG. 7. (a) Plot of the average $\bar{K}_{\text{trans}}$ from Fig. 6 as a function of magnetic field. Data color indicates the various neutral pressures, and open and closed circles represent electrode biases of +40 and −40 V, respectively. The average $\bar{K}_{\text{trans}}$ is typically much lower with increased neutral pressure, though all cases show similar systematic trends with magnetic field. (b) Ratios of the standard deviation of kinetic energy over time δK to $\bar{K}_{\text{trans}}$ are shown as percentages. While higher neutral pressure is indicative of a decreased $\bar{K}_{\text{trans}}$, here it is shown that for those same cases the standard deviation relative to the mean is much higher. For lower pressures this ratio is generally less than 10%.

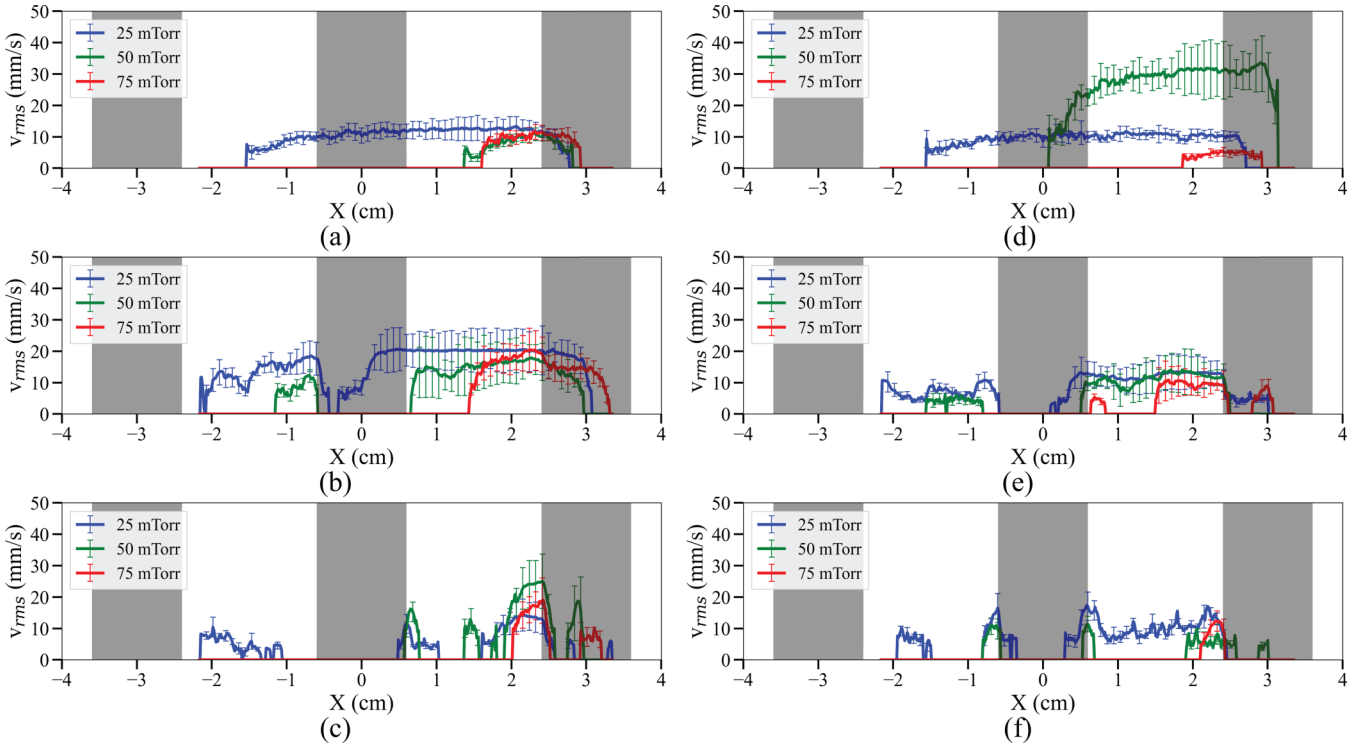

FIG. 8. Root mean square velocity profiles for magnetic fields (a) and (d) $B = 0.0$ T, (b) and (e) $B = 1.02$ T, and (c) and (f) $B = 2.05$ T and waffle electrode biases of (a)–(c) $V = -40$ V and (d)–(f) $V = +40$ V. Neutral gas pressures of 25 mTorr (3.33 Pa) are shown in blue, 50 mTorr (6.67 Pa) in green, and 75 mTorr in red. The position of the waffle electrode is shown as vertical gray bands.

square velocities are shown for various neutral pressures, magnetic fields, and waffle electrode biases. These profiles in the x direction are determined from taking an average in the y direction within the dashed outline regions illustrated in Fig. 5 and described at the end of the preceding section. These profiles provide a clear representation of the particle positions beneath the waffle electrode and the typical velocities of those particles.

In the absence of an applied magnetic field [Figs. 8(a) and 8(d)] the $v_{\rm rms}$ profiles extend across the waffle electrode region, indicative of a single dust cloud in this region. Some differences are found to be a function of neutral pressure, or electrode bias. These differences are expected, such as reduced velocities, which are likely due to damping at higher neutral pressures. In the presence of some moderate amount of magnetic field $B = 1.02$ T [Figs. 8(b) and 8(e)], the dust cloud is found to primarily reside beneath the holes of the waffle electrode, especially at neutral pressures of $P =$ 25 mTorr (3.33 Pa). At a bias of $V = -40$ V [Fig. 8(b)], the cloud extends further beneath the conducting elements, indicating some dependence on electrode bias. At the highest magnetic field conditions $B = 2.05$ T [Figs. 8(c) and 8(f)], the dust clouds which spanned the width of the hole region appear to decompose further into smaller groupings of particles located at the edges of the hole region. While the higher magnetic fields appear to limit the occupiable space within the plasma for the dust particles, they do not appear to affect the $v_{\rm rms}$ of the particles, as the profiles show little change in magnitude with magnetic field. Instead the neutral pressure appears to have the more direct effect on velocities, regardless of whether an applied magnetic field is present.

This result is also significant in that it shows that the dust clouds appear to aggregate in regions where the plasma glow is the most intense. In Fig. 9 images of the average intensity of the plasma glow beneath the waffle electrode are presented. Two example images of the plasma glow are shown at magnetic fields of 0.0 T [Fig. 9(a)] and 1.02 T [Fig. 9(b)] for a neutral pressure of 25 mTorr (3.33 Pa) and waffle electrode bias of −40 V. These images are formed from the average pixel intensities of 100 video frames with dimensions of 1928×1770 pixels and spatial resolution of 24 μm/pixel. These videos were recorded separately from the dust video recordings when no dust was present in the experiment. When there is no magnetic field the plasma is found to be uniform with no prominent change in the glow around the electrode. However, in the presence of a strong magnetic field the plasma glow around the electrode is found to be heavily modified with enhanced plasma glow beneath the holes of the electrode and a sharp transition between those regions and the areas beneath the conductor.

Intensity profiles of the plasma glow are also shown for these same conditions, with the addition of the +40-V electrode bias. These profiles are an average in the y direction of the red highlighted region in the average intensity images. This region is located a distance of 2.5 cm below the waffle electrode, about 5 cm above the location where the dust levitates. At $B = 0.0$ T these profiles show a very uniform plasma glow and appear similar to the $v_{\rm rms}$ profiles at similar conditions. At high magnetic fields $B = 1.02$ T, the development of an increased plasma glow beneath the holes of the electrode is observed for both positive and negative electrode biases. When the potential is positive, the plasma is brightest

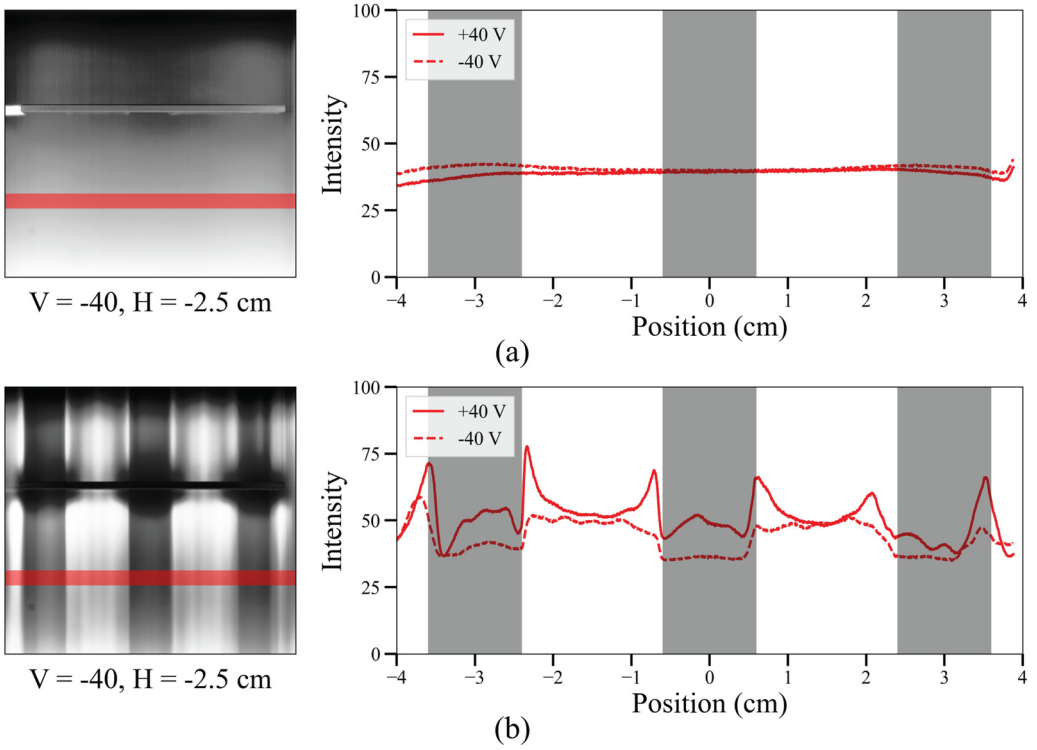

FIG. 9. Average light intensity images and light intensity profiles beneath the waffle electrode at (a) $B = 0.0\ T$ and (b) $B = 1.02$ T, with both at a neutral press of 25 mTorr. An enhanced plasma glow beneath the holes of the waffle electrode can be observed in the average intensity images. The intensity profiles are taken from a vertical average within the red highlighted region in the average intensity images, a 100-pixel-high area centered 2.5 cm below the waffle electrode. For $B = 0.0\ T$ the intensity profiles are effectively uniform beneath the electrode and show no difference with electrode bias. At $B = 1.02\ T$ the profiles show an increase in the intensity beneath the holes, developing a two-peak structure at an electrode bias of +40 V which is similar to the v_{rms} profiles under similar conditions.

at the edges of the electrode holes, much like how the confined dust particles are drawn to these same edge regions. One explanation for this correlation is that the dust particles are attracted to regions which contain plasma filaments, seen as vertical striations within Fig. 9(b).

In the presence of high magnetic fields, low-temperature and dusty plasmas have been observed to develop patterned structures within the plasma, which have been termed filaments [29]. These filament structures are observed as a variety of patterns such as columns, spirals, or concentric rings, depending on the plasma conditions, and continue to be an area of active research [30–32].

While the particles appear to be attracted to regions within the plasma which contain these plasma filaments, this raises the question as to whether these filaments act as a source of energy by which the dust particles maintain their steady state. By viewing the experiment from above, along the magnetic axis, it is possible to examine the fluctuations of the plasma within the holes of the waffle electrode. In Fig. 10(a) a top-down image of the waffle electrode is shown. Here some dust particles can be seen beneath the holes of the electrode, most notably in the lower half. For reference, the side camera views this region from the left. By averaging the pixel intensity in the yellow-boxed region, a simple measure of the plasma glow fluctuation can be made over time. The results of a small sample of this measurement are shown in Fig. 10(b). This plot shows that for various magnetic fields, at a neutral pressure of 25 mTorr and bias of −40 V, the plasma glow is brighter and has slightly more fluctuations when the applied magnetic field is present. This is consistent with the results from Fig. 9.

When this intensity is time averaged and plotted as a function of magnetic field, as is done in Fig. 10(c), behavior is found similar to the one seen in Fig. 7(a). In both plots a peak in the mean intensity or kinetic energy is found at $B = 0.51$ T and then steadily decreasing with magnetic field. This suggests that the increase in dust energy is somehow tied to the brighter plasma glow, which itself is likely due to the increased plasma density in the hole regions [33], also meaning that an energy source for the dust particles is unlikely to arise from the fluctuations within the plasma itself. Figure 10(d) plots the ratio of the standard deviation of the light intensity over time to the time-averaged light intensity. Where it was the case that the kinetic energy and intensity peak at 0.51 T, this ratio experiences a minimum at this same field strength, meaning there is no significant increase in the light fluctuation which could be correlated to the increase in dust energy. While the particles do aggregate and receive an increase in energy from a possible superfilament of plasma within the hole of the waffle electrode, the dust particles do not appear to experience other effects from smaller filaments which produce smaller fluctuations within the same space.

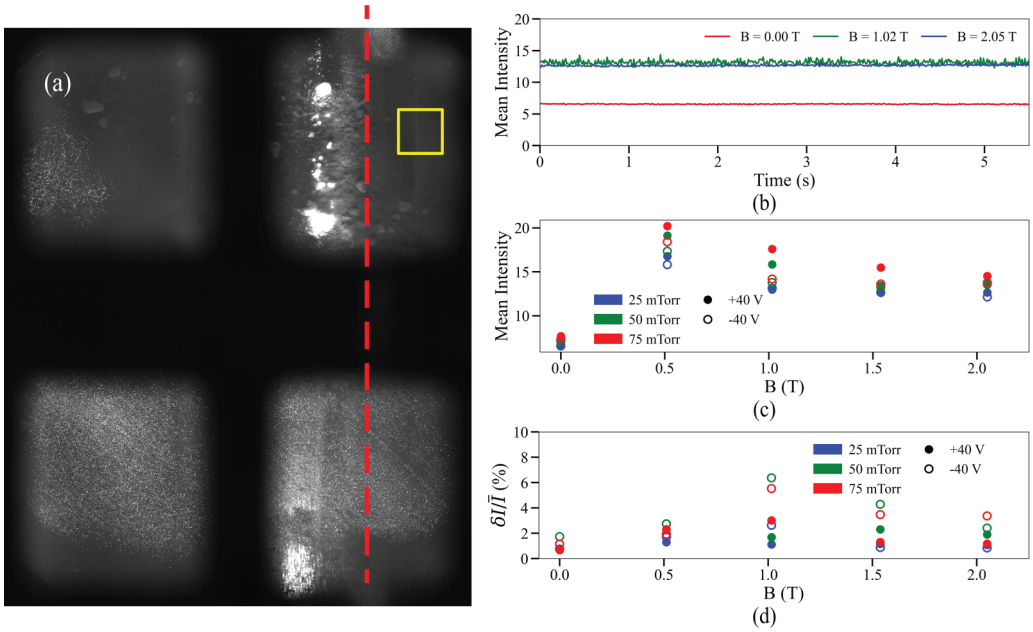

FIG. 10. (a) Top down image from maximum pixel intensities over 100 image frames. Experimental conditions are $B = 1.02$ T, $P = 25$ mTorr, and a waffle electrode bias of $V = -40$ V. The yellow square is the region for calculating the average pixel intensity within each image. The red dashed line represents the vertical laser sheet intersecting the waffle electrode for the images in Fig. 3. (b) Mean pixel intensity within the yellow box over time, which shows that the pixel intensity is increased at higher magnetic fields and has a larger degree of fluctuation. All three magnetic field cases are at a neutral gas pressure of 25 mTorr (3.33 Pa) and waffle electrode bias of $V = -40$ V. (c) Time-averaged pixel intensity plotted versus magnetic field. In the presence of an applied magnetic field, the intensity increases to roughly 2–3 times the value of the no magnetic field case. (d) Plot of the relative error of the time-averaged pixel intensity. The largest relative fluctuations occur at around $B = 1.02$ T and appear to increase with higher neutral pressure.

V. SUMMARY

The investigation into pattern formation in low-temperature and dusty plasmas in the presence of high magnetic fields is a relatively new area of research which has developed in the past decade. This research is highly focused on the physics of imposed ordered structures and continues to examine these imposed ordered structures by use of a new waffle-shaped electrode.

The experimental observations of the dust and the plasma glow show that, with increasing magnetic field, there is an apparent restriction of the plasma and particles to regions beneath the holes of the waffle electrode holes. From these observations, three primary conclusions are drawn. The first is a possible answer to the question regarding the location of the dust particles beneath the conducting element which produces the imposed ordered structure. By using the new waffle-shaped electrode it can be easily observed that the dust resides beneath the holes and not the conductor surface of this new electrode. Whether these effects remain the same when the conducting hardware is scaled back down to the size of the wire mesh still requires further investigation. The second is that the dust particles exist in an energetic steady state, regardless of magnetic field. By using PIV to measure root mean square velocities, a measure of the kinetic energy is made over time, showing no indications of energy growth or decay.

The third result is that the particles become trapped in regions of increased plasma glow. This result is supported by observations of the plasma glow around the waffle electrode which show that the plasma glow beneath the waffle electrode is highly modified by the waffle electrode at high magnetic fields. The locations of the peaks in plasma glow intensity strongly correspond to the v_{rms} profiles determined from observations of the dust particles. Measurements of the plasma glow fluctuations show that an increase in the plasma glow brightness is associated with the increase in dust kinetic energy, but that fluctuations in the light intensity are not, meaning that small plasma filaments are not a likely source of energy for maintaining the energetic steady state. However, it may be that the bright column of plasma through the hole of the waffle electrode is itself a superfilament which traps the dust particles and influences their overall energy.

As an additional observation, which goes beyond the scope of this work but may serve as motivation for future work, is that the v_{rms} profiles and plasma glow intensity profiles are found to have a steep slope at the electrode edges. This sharp potential gradient is highly suggestive of the formation of a plasma sheath, which traditionally forms near boundaries within the plasma such as the edges of the electrode [34,35]. Here these sharp gradients appear to extend far into the bulk plasma, being observed both in the plasma glow around waffle electrode and in the dust v_{rms} profiles. A follow-up paper examining the relationship between the imposed ordered structures and plasma filaments should help to provide more information on the relationship between these two interesting phenomena [36].

However, some further questions still remain. The most outstanding of these questions comes from the fact that the waffle electrode is significantly larger than the wire mesh used in previous experiments. In those systems the wire diameter and hole spacing in the mesh were often on the order of a few hundred microns, which is the approximate scale of the plasma Debye length. The conducting bands of the waffle electrode and the gaps between them are now on the order of 1 cm, several hundred times larger. How the imposed ordered structures scale with the size of the wire or hole spacing is still not well understood and future experiments will need to be conducted to determine an answer.

ACKNOWLEDGMENTS

This material was based upon the work supported by the U.S. Department of Energy, Grants No. DE-SC0016330 and No. SC-0019176, and by the National Science Foundation, Grant No. PHY-1613087. The construction of the MDPX device was funded through the NSF Major Research Instrumentation program, Grant No. PHY-1126067. Additional support was provided by the NSF EPSCoR program (Cooperative Agreement No. OIA-1655280). The authors would also like to thank all the members of the MDPX research team whose advice and suggestions have been invaluable in the pursuit of this project.

[1] P. K. Shukla, Phys. Plasmas **8**, 1791 (2001).
[2] P. K. Shukla and A. A. Mamun, *Introduction to Dusty Plasma Physics* (Institute of Physics, Bristol, 2002).
[3] A. Piel, *Plasma Physics* (Springer, Berlin, 2010).
[4] J. Goree, Plasma Sources Sci. Technol. **3**, 400 (1994).
[5] E. Thomas and M. Watson, Phys. Plasmas **7**, 3194 (2000).
[6] S. Khrapak and G. Morfill, Contrib. Plasma Phys. **49**, 148 (2009).
[7] E. Thomas, B. Lynch, U. Konopka, R. L. Merlino, and M. Rosenberg, Phys. Plasmas **22**, 030701 (2015).
[8] E. Thomas, U. Konopka, B. Lynch, S. Adams, S. LeBlanc, R. L. Merlino, and M. Rosenberg, Phys. Plasmas **22**, 113708 (2015).
[9] T. Hall, E. Thomas, K. Avinash, R. Merlino, and M. Rosenberg, Phys. Plasmas **25**, 103702 (2018).
[10] E. Thomas, A. M. Dubois, B. Lynch, S. Adams, R. Fisher, D. Artis, S. Leblanc, U. Konopka, R. L. Merlino, and M. Rosenberg, J. Plasma Phys. **80**, 803 (2014).
[11] E. Thomas, U. Konopka, D. Artis, B. Lynch, S. Leblanc, S. Adams, R. L. Merlino, and M. Rosenberg, J. Plasma Phys. **81**, 345810206 (2015).
[12] R. L. Merlino, E. Thomas, B. Lynch, S. LeBlanc, T. Hall, U. Konopka, and M. Rosenberg, in *Non-Neutral Plasma Physics X: 12th International Workshop on Non-Neutral Plasmas, Appleton, 2017*, edited by M. R. Stoneking, AIP Conf. Proc. No. 1928 (AIP, Melville, 2018), p. 020011.
[13] E. O. Johnson and L. Malter, Phys. Rev. **80**, 58 (1950).
[14] F. F. Chen, Rev. Sci. Instrum. **35**, 1208 (1964).
[15] A. Barkan, N. D'Angelo, and R. L. Merlino, Phys. Rev. Lett. **73**, 3093 (1994).
[16] E. Thomas, Phys. Plasmas **8**, 329 (2001).
[17] E. Thomas, Phys. Plasmas **9**, 17 (2002).
[18] M. Puttscher, A. Melzer, U. Konopka, S. LeBlanc, B. Lynch, and E. Thomas, Phys. Plasmas **24**, 013701 (2017).
[19] 1003001_DaVis_D81_manual, Product Manual for DaVis 8.1 Software (LaVision, Göttingen, 2013).
[20] J. D. Williams and E. Thomas, Phys. Plasmas **14**, 063702 (2007).
[21] E. Thomas, J. Williams, and C. Rath, IEEE Trans. Plasma Sci. **38**, 892 (2010).
[22] E. Thomas, Phys. Plasmas **6**, 2672 (1999).
[23] E. Thomas, J. D. Williams, and J. Silver, Phys. Plasmas **11**, L37 (2004).
[24] E. Thomas, Jr. and J. Williams, Phys. Plasmas **13**, 055702 (2006).
[25] Z. Aldewereld and E. Thomas, IEEE Trans. Plasma Sci. **35**, 309 (2007).
[26] R. Fisher and E. Thomas, Phys. Plasmas **18**, 113701 (2011).
[27] S. A. Khrapak, A. V. Ivlev, G. E. Morfill, and H. M. Thomas, Phys. Rev. E **66**, 046414 (2002).
[28] C. Zafiu, A. Melzer, and A. Piel, Phys. Plasmas **9**, 4794 (2002).
[29] M. Schwabe, U. Konopka, P. Bandyopadhyay, and G. E. Morfill, Phys. Rev. Lett. **106**, 215004 (2011).
[30] E. Thomas, U. Konopka, R. L. Merlino, and M. Rosenberg, Phys. Plasmas **23**, 055701 (2016).
[31] M. Menati, E. Thomas, and M. J. Kushner, Phys. Plasmas **26**, 063515 (2019).
[32] E. E. Thomas, B. R. Lynch, U. Konopka, M. Menati, S. A. Williams, R. L. Merlino, and M. Rosenberg, Plasma Phys. Control. Fusion **62**, 014006 (2020).
[33] T. H. Hall, Microparticle dynamics in the presence of externally imposed, ordered structures in a magnetized, low-temperature plasma, Ph.D. thesis, Auburn University, 2019, http://etd.auburn.edu/handle/10415/6998.
[34] K. U. Riemann, J. Phys. D **24**, 493 (1991).
[35] N. Hershkowitz, Phys. Plasmas **12**, 055502 (2005).
[36] M. Menati, T. Hall, B. Rasoolian, L. Couedel, E. Thomas, and U. Konopka, Plasma Sources Sci. Technol. (2020), doi:10.1088/1361-6595/aba7ed.